Acta Crystallographica Section D
Biological Crystallography
ISSN 1399-0047

The structure of human interleukin-11 reveals receptor-binding site features and structural differences from interleukin-6

Tracy L. Putoczki,[a,b] Renwick C. J. Dobson[c,d] and Michael D. W. Griffin[d]*

[a]Inflammation Division, Walter and Eliza Hall Institute of Medical Research, Parkville, Victoria 3052, Australia, [b]Department of Medical Biology, University of Melbourne, Parkville, Victoria 3010, Australia, [c]Biomolecular Interactions Centre and School of Biological Sciences, University of Canterbury, Private Bag 4800, Christchurch 8020, New Zealand, and [d]Department of Biochemistry and Molecular Biology, Bio21 Molecular Science and Biotechnology Institute, University of Melbourne, Parkville, Victoria 3010, Australia

Correspondence e-mail: mgriffin@unimelb.edu.au

Received 3 April 2014
Accepted 27 May 2014

PDB reference: human interleukin-11, 4mhl

Interleukin (IL)-11 is a multifunctional member of the IL-6 family of cytokines. Recombinant human IL-11 is administered as a standard clinical treatment for chemotherapy-induced thrombocytopaenia. Recently, a new role for IL-11 signalling as a potent driver of gastrointestinal cancers has been identified, and it has been demonstrated to be a novel therapeutic target for these diseases. Here, the crystal structure of human IL-11 is reported and the structural resolution of residues previously identified as important for IL-11 activity is presented. While IL-11 is thought to signal *via* a complex analogous to that of IL-6, comparisons show important differences between the two cytokines and it is suggested that IL-11 engages GP130 differently to IL-6. In addition to providing a structural platform for further study of IL-11, these data offer insight into the binding interactions of IL-11 with each of its receptors and the structural mechanisms underlying agonist and antagonist variants of the protein.

1. Introduction

Interleukin (IL)-11 is secreted by a number of different cell types, resulting in a broad range of biological activities *in vivo*. Early studies identified a role for IL-11 as a haematopoietic growth factor (Du & Williams, 1997; Schwertschlag *et al.*, 1999; reviewed in Putoczki & Ernst, 2010), with a particular focus on its thrombopoietic activity. As a result, the US Food and Drug Administration has approved the use of recombinant human (h)IL-11 (oprelvekin, Neumega) for the treatment of severe thrombocytopaenia in patients undergoing myelosuppressive chemotherapy. The administration of recombinant hIL-11 has also undergone clinical trials for Crohn's disease (Herrlinger *et al.*, 2006; Sands *et al.*, 2002), following the success of exogenous administration of the cytokine in alleviating epithelial damage and chronic inflammation in animal models of intestinal injury and inflammatory bowel disease (Peterson *et al.*, 1998; Qiu *et al.*, 1996). Current clinical and biochemical efforts are now focused on improving the therapeutic efficacy of recombinant hIL-11 through the design of agonist variants of the protein (Dams-Kozlowska *et al.*, 2013).

IL-11 belongs to the IL-6 family of cytokines, which includes IL-6, leukaemia inhibitory factor, ciliary neurotrophic factor, oncostatin M, cardiotrophin-1, IL-27 and IL-31 (Taga & Kishimoto, 1997). Traditionally, IL-6 has been linked to chronic inflammatory diseases and the progression of numerous cancers, including gastrointestinal (GI) cancers, through its activation of the signal transducer and activator of transcription 3 (STAT3) pro-survival pathway. As a result, the structure of the IL-6 signalling complex has been thoroughly

Table 1
X-ray data-collection and structure-refinement statistics for hIL-11.

Values in parentheses are for the highest resolution shell.

Data collection	
Space group	$P2_12_12$
Wavelength (Å)	0.9537
No. of images	100
Oscillation range per image (°)	1.0
Detector	ADSC Quantum 315r
Unit-cell parameters (Å, °)	a = 118.86, b = 28.17, c = 41.81, $\alpha = \beta = \gamma = 90$
Resolution (Å)	41.81–2.09 (2.15–2.09)
$R_{\rm merge}$†	0.090 (0.459)
$R_{\rm meas}$‡	0.120 (0.611)
$R_{\rm p.i.m.}$§	0.079 (0.400)
$\langle I/\sigma(I)\rangle$	11.5 (2.9)
Total observations	34068
Unique reflections	8862
Completeness (%)	99.6 (97.5)
Multiplicity	3.8 (3.8)
Wilson B factor (Å^2)	29.40
Matthews coefficient $V_{\rm M}$ (Å^3 Da^{-1})	1.84
Solvent content (%)	33.1
Refinement	
Resolution (Å)	41.81–2.09 (2.14–2.09)
Reflections used in refinement	8203 (584)
$R_{\rm free}$ reflections	624 (45)
$R_{\rm work}$	0.184 (0.199)
$R_{\rm free}$	0.242 (0.259)
Protein molecules in asymmetric unit	1
Protein residues	161
No. of atoms	
Total	1309
Protein	1214
Ligand/ion	20
Water	75
Mean B factors (Å^2)	
Overall	30.35
Protein	30.08
Ligand/ion	31.61
Water	34.33
R.m.s. deviations	
Bond lengths (Å)	0.009
Bond angles (°)	1.39

† $R_{\rm merge} = \sum_{hkl}\sum_i |I_i(hkl) - \langle I(hkl)\rangle| / \sum_{hkl}\sum_i I_i(hkl)$. ‡ $R_{\rm meas} = \sum_{hkl}\{N(hkl)/[N(hkl)-1]\}^{1/2}\sum_i |I_i(hkl) - \langle I(hkl)\rangle| / \sum_{hkl}\sum_i I_i(hkl)$. § $R_{\rm p.i.m.} = \sum_{hkl}\{1/[N(hkl)-1]\}^{1/2}\sum_i |I_i(hkl) - \langle I(hkl)\rangle| / \sum_{hkl}\sum_i I_i(hkl)$.

investigated and used to guide the design of antagonizing antibodies that are now in routine use for rheumatoid arthritis (Tanaka *et al.*, 2012) and are in clinical trials for numerous cancers (Yao *et al.*, 2014). We have recently demonstrated that while both IL-6 and IL-11 are elevated in GI cancers, IL-11 has a stronger correlation with STAT3 activation (Putoczki *et al.*, 2013). Using mouse genetic models, we confirmed that IL-11 has a more prominent role than IL-6 during the progression of GI cancers. Importantly, we showed that an antagonist variant of IL-11 effectively inhibits STAT3 activation and suppresses the invasive capacity and growth of tumours in human cell-line xenograft models (Putoczki *et al.*, 2013). These results suggest that IL-11 has biological functions that dominate over its well characterized sibling IL-6.

IL-11 is a member of the superfamily of long helical cytokines, which are structurally characterized by a four-helix bundle motif comprising two pairs of antiparallel α-helices in an up–up–down–down configuration. Signalling by IL-11 proceeds *via* interaction of the protein with its membrane-anchored specific receptor IL-11Rα and the subsequent engagement of this dimer by the transmembrane signal-transducing receptor GP130 (also called IL6ST). With the exception of IL-31, the IL-6 family of cytokines are characterized by their shared use of GP130, in addition to their cytokine-specific cell-surface receptors. Previous models of the IL-11 signalling complex were based on the crystal structure of the human IL-6 signalling complex (Boulanger, Chow *et al.*, 2003), which comprises a hexamer of IL-6, IL-6Rα and GP130 in a 2:2:2 stoichiometry. Biochemical studies and low-resolution cryo-electron microscopy have confirmed that the functional IL-11 signalling complex is also hexameric, comprising two molecules each of IL-11, IL-11Rα and GP130 (Barton *et al.*, 2000; Matadeen *et al.*, 2007). In the light of these observations, the mechanism of IL-11 signalling has been described as analogous to that of IL-6. However, mature IL-11 shares only 18% sequence identity with IL-6, and distinct biological activities of the two cytokines have been well documented (reviewed in Garbers & Scheller, 2013; Putoczki & Ernst, 2010).

Given the new and diverging roles for IL-11 in disease together with the exciting treatment options that this knowledge affords, a more detailed understanding of the structure and formation of the IL-11 signalling complex is necessary. Here, we report the crystal structure of hIL-11 coupled with solution-structure analysis, and relate these data to both structure–function studies of IL-11 activity and crystal structures of IL-6. The structure of hIL-11 resolves the positions of specific residues critical for receptor binding and identifies the regions of the protein responsible for binding to each of its receptors. Structural comparisons of IL-11 with IL-6 indicate important differences and suggest that IL-11 binds to the primary molecule of GP130 *via* a different binding mode and/or an alternative GP130 binding site to IL-6. Our findings provide a structural platform that will guide the design of future agonist and antagonist variants of IL-11 and highlight differences between IL-11 and IL-6 that may define their biological activities.

2. Materials and methods

2.1. Crystallization and X-ray diffraction data collection

Human IL-11 (hIL-11) produced recombinantly in *Escherichia coli* as described by Czupryn *et al.* (1995) was used throughout. This protein construct comprises residues 23–199 of the hIL-11 precursor sequence, omitting the N-terminal proline residue (Pro22) of mature hIL-11. hIL-11 was crystallized using the sitting-drop vapour-diffusion method in 24-well Cryschem plates. Crystals of approximate dimensions 5 × 5 × 150 µm were obtained at 293 K from crystallant consisting of 1.25 *M* ammonium sulfate, 200 m*M* lithium sulfate, 100 m*M* bis-tris propane, 10–14%(*v*/*v*) formamide pH 9.5. Crystallization drops were produced by adding 1.5 µl crystallant to 1.5 µl 10 mg ml^{-1} hIL-11 in 20 m*M* Tris–HCl pH 7.4. Crystals appeared after equilibration against crystallant

for 4–6 weeks and continued to grow for a further 2–4 weeks. Crystals were flash-cooled in liquid nitrogen directly from the crystallization drop and X-ray diffraction intensity data collection was carried out at 100 K on the MX2 beamline at the Australian Synchrotron.

2.2. Phasing and model refinement

Diffraction data were indexed and integrated using *XDS* (Kabsch, 2010) and were analysed using *POINTLESS* (Evans, 2011) before scaling and merging using *AIMLESS* (Evans & Murshudov, 2013) from the *CCP*4 suite (Winn *et al.*, 2011). Initial phase estimates were obtained by molecular replacement using *Phaser* (McCoy *et al.*, 2007) with modified coordinates from the crystal structure of IL-6 (PDB entry 1alu; Somers *et al.*, 1997) as the search model. This strategy provided a number of weak solutions that were manually edited to facilitate further refinement. Structure refinement was performed using *REFMAC*5 (Murshudov *et al.*, 2011) with iterative building, model corrections and addition of solvent molecules using *Coot* (Emsley *et al.*, 2010). Three cycles of simulated annealing using *PHENIX* (Adams *et al.*, 2010) were performed at an early stage of the refinement to minimize model bias. Translation/libration/screw (TLS) refinement was performed with *REFMAC*5 in the final rounds of refinement using a single TLS group containing all protein atoms. The crystals of hIL-11 belonged to space group $P2_12_12$ with an asymmetric unit composed of one protein molecule, and the crystal structure was refined to a resolution of 2.09 Å (Table 1). The crystal structure comprises residues 34–81, 84–151 and 155–199 of hIL-11. Residues Ser81–Ala84 lie close to a twofold symmetry axis, and no continuous density was available for modelling of Ala82–Gly83. Weak continuous density allowed backbone tracing of residues Pro150–Gln151 and Asp155–Leu161 (Supplementary Fig. S1[1]), and these residues were included in the model. However, poorly defined density in these regions resulted in minor backbone distortions during refinement, placing Leu161 slightly outside the Ramachandran allowed regions. Side chains were omitted from the structure in positions where insufficient electron density was available to guide rotamer building. Formamide molecules were placed in appropriate elongated solvent-density peaks that could not be modelled accurately with water molecules. Secondary-structure assignments were carried out with *DSSP* (Kabsch & Sander, 1983). Structural alignment was performed with *SUPERPOSE* from the *CCP*4 suite. Surface electrostatics were evaluated using the *Adaptive Poisson–Boltzmann Solver* (*APBS*) software (Baker *et al.*, 2001) in *PyMOL* after replacement of the side-chain atoms that had been omitted from the model. Theoretical sedimentation coefficients and maximum interatomic distances were calculated from the crystal structure coordinates using *HYDROPRO* (Ortega *et al.*, 2011) under the experimental conditions described in §2.3.

[1] Supporting information has been deposited in the IUCr electronic archive (Reference: CB5059).

2.3. Analytical ultracentrifugation

Sedimentation-velocity experiments were performed in a Beckman Coulter Model XL-I analytical ultracentrifuge equipped with UV–Vis scanning optics. Reference (400 µl 20 m*M* Tris–HCl, 150 m*M* NaCl pH 7.4) and sample (380 µl) solutions were loaded into 12 mm double-sector cells with quartz windows and the cells were mounted in an An-60 Ti four-hole rotor. hIL-11 was centrifuged at concentrations of 0.2, 0.6 and 1.0 mg ml^{-1} at 50 000 rev min^{-1} (201 600*g*) and 20°C. Radial absorbance data were collected at 280 nm in continuous mode every 10 min. Sedimentation data were fitted to a continuous sedimentation-coefficient distribution [$c(s)$] model using *SEDFIT* (Schuck, 2000). The partial specific volume of hIL-11 (0.7511 ml g^{-1}), the buffer density (1.005 g ml^{-1}) and buffer viscosity (1.021 cP) were calculated using *SEDNTERP* (Laue *et al.*, 1992). Molecular weight was calculated with *SEDFIT* from the experimental sedimentation coefficient and using a frictional ratio (f/f_0) of 1.31 estimated from the fit to sedimentation-velocity data obtained at 1.0 mg ml^{-1} hIL-11.

2.4. Small-angle X-ray scattering data collection and analysis

Small-angle X-ray scattering (SAXS) data were collected on the SAXS/WAXS beamline at the Australian Synchrotron. The sample-to-detector distance was 1480 mm and the X-ray beam energy was 11 000 eV (λ = 1.12713 Å), providing a total s range of 0.011–0.566 Å^{-1}. Scattering data were collected from a 1.5 mm glass capillary at 10°C under continuous flow (0.2 ml min^{-1}) with 2 s frames. hIL-11 (10 mg ml^{-1}) was eluted directly into the capillary from an in-line Superdex 200 5/150 size-exclusion column (GE Healthcare) pre-equilibrated with 20 m*M* HEPES, 150 m*M* NaCl pH 7.4. Scattering images collected during hIL-11 elution were radially averaged, normalized to sample transmission and background-subtracted. Data were analysed using the *ATSAS* software suite (Petoukhov *et al.*, 2012); they showed no indication of sample aggregation and the Guinier plots were linear for $s \cdot R_g < 1.3$ (Supplementary Fig. S2). The theoretical scattering curve was calculated from the refined hIL-11 crystal structure coordinates using *CRYSOL* (Svergun *et al.*, 1995). The pair distance distribution function, $P(r)$, was calculated by indirect Fourier transform using *GNOM* (Svergun, 1992).

2.5. Data deposition

Coordinates and structure factors have been deposited in the Protein Data Bank as entry 4mhl. SAXS data and the $P(r)$ profile have been deposited in the BIOISIS database as entry HIL11P.

3. Results and discussion

3.1. The crystal structure of human IL-11

Despite significant attention over several decades, the high-resolution structure of IL-11 has not been reported and structure–function studies of IL-11 have largely been based

on homology models using other long-helical and IL-6 family cytokines. Accordingly, we solved the crystal structure of hIL-11 to provide a definitive structural model of IL-11.

The structure of hIL-11 comprises a typical type-1 cytokine four-helix bundle in an up–up–down–down configuration (Fig. 1; PDB entry 4mhl). The long loop between helix A and helix B (loop AB) was largely well defined in the electron density, except for residues Ala82 and Gly83. This loop lies primarily across the surface of helix B and helix D and makes numerous specific contacts with these helices. In contrast, electron density for loop CD was generally weak, indicating significant disorder of this region. Despite this, continuous electron density allowed backbone tracing of loop CD residues Leu147–Gln151 and Asp155–Ser166 (Supplementary Fig. S1). These two large loops were both situated facing towards a large solvent-filled channel in the crystal and do not participate significantly in crystal contacts, suggesting that their general conformation in the crystal is representative of their conformation in solution.

3.2. Solution structure analysis of hIL-11

To complement the crystal structure, solution studies of hIL-11 were conducted to assess the solution structural and biophysical properties of the protein. The oligomeric state of hIL-11 was investigated using sedimentation-velocity analytical ultracentrifugation at concentrations of 0.2, 0.6 and 1.0 mg ml^{-1} (Supplementary Fig. S2). Continuous sedimentation-coefficient distributions show a single large peak with a modal sedimentation coefficient of approximately 1.7 S (Fig. 2*a*). This sedimentation coefficient corresponds to an approximate molecular weight of 19 kDa assuming an f/f_0 of 1.31, which was calculated from data obtained at 1 mg ml^{-1} hIL-11. This is in good agreement with the calculated molecular weight of 19 047 Da for hIL-11. Calculation of the theoretical sedimentation coefficient from the crystal structure of hIL-11 yields a monomer sedimentation coefficient of 1.82 S, providing further evidence that this peak in the $c(s)$ distribution corresponds to a monomeric form of hIL-11. At higher concentrations of hIL-11, a small peak around 3.2 S became apparent that may correspond to an oligomeric form of the protein, possibly a dimer. However, given that physiological concentrations of IL-11 are significantly lower than those investigated here, it is likely that the active form of hIL-11 *in vivo* is monomeric.

To verify the solution conformation of hIL-11, the protein was further characterized by SAXS. Experimental data showed good agreement with the theoretical scattering profile calculated from the monomeric crystal structure coordinates (Fig. 2*b*), indicating low structural plasticity of the helical bundle motif and little oligomeric self-association of the

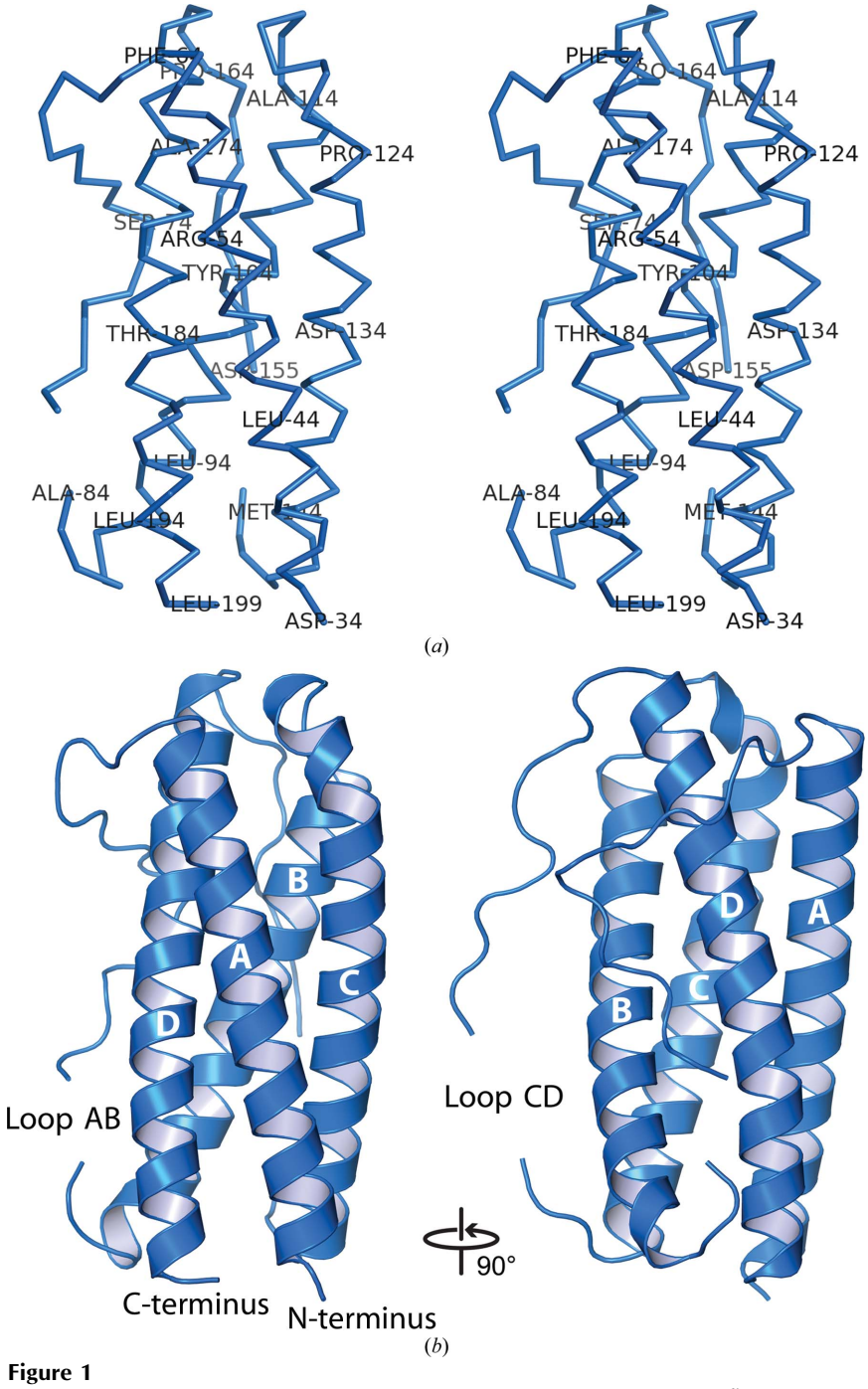

Figure 1
The crystal structure of hIL-11. (*a*) Wall-eye stereo representation of the C$^{\alpha}$ backbone of hIL-11. Residue numbering is provided according to the full-length precursor sequence of hIL-11. (*b*) Schematic representation of the secondary structure of hIL-11 indicating helix and loop naming.

protein under these conditions. The maximum dimension of the scattering particle (D_{max}) was approximately 62.5 Å (Supplementary Fig. S2), which is larger than the maximum interatomic dimension of the crystal structure of 58.8 Å. This discrepancy may be owing to the dynamic nature of the large loops of hIL-11 or the presence of 11 N-terminal residues that were disordered in the crystal and were not included in the model. The approximate molecular weight calculated from this analysis was 18.2 kDa, which is in close agreement with the expected monomeric weight of the protein. Taken together, these solution studies closely match our crystallographic model and suggest a stable monomeric structure for hIL-11.

3.3. Receptor-binding regions of IL-11

Mutagenic studies of both human (Harmegnies *et al.*, 2003; Tacken *et al.*, 1999) and mouse (Barton *et al.*, 1999; Underhill-Day *et al.*, 2003) IL-11 have been undertaken to define the residues that are involved in function. It is possible to map all of these residues onto the crystal structure of hIL-11 owing to the high homology between human and mouse IL-11 (87.6%) and the conservation in hIL-11 of each of the residues studied in the mouse protein (Fig. 3; for a sequence alignment, see Supplementary Fig. S3). This analysis demonstrates that the residues involved in signalling reside on all four helical elements and the C-terminal end of loop AB. These residues can be divided into three groups based on evidence that each mediates binding of IL-11 to IL-11Rα (referred to as site I), to the first molecule of GP130 (site II) or to the second molecule of GP130 (site III; see also Supplementary Fig. S4). For example, Arg190 lies on helix D, with mutation of this residue to alanine in mouse IL-11 and to glutamate in human IL-11 resulting in dramatic attenuation of binding to the respective α-receptors (Barton *et al.*, 1999; Tacken *et al.*, 1999), indicating that this site forms an essential contact with IL-11Rα at site I. In contrast, mutation of both Arg132 and Leu136 to alanine in mouse IL-11 resulted in slightly increased affinity for IL-11Rα but significantly reduced signalling activity, suggesting that this region of the protein is primarily involved in binding to the first molecule of GP130 *via* site II (Barton *et al.*, 1999). Residues that participate in the interaction of IL-11 with the second GP130 molecule, mediating formation of the complete hexameric signalling complex (site III), are located at the end of the helical bundle distal to sites I and II. Interestingly, the single mutation W168A within this cluster results in an antagonist that can competitively inhibit wild-type IL-11 signalling (Underhill-Day *et al.*, 2003) while having little effect on the affinity for IL-11Rα (Barton *et al.*, 1999). The antagonist activity of this mutant protein appears to arise from its ability to disrupt formation of the functional hexameric assembly.

A higher potency IL-11 antagonist was developed based on the W168A mutation by screening targeted libraries for variants with increased affinity for IL-11Rα (Lee *et al.*, 2008). This high-potency IL-11 antagonist is a variant of mouse IL-11 that contains five continuous substitutions at positions 79–83, AMSAG→PAIDY, in the region of site I coupled with the W168A mutation (Lee *et al.*, 2008). These mutations result in binding of this variant to IL-11Rα with a 20-fold higher affinity than wild-type mouse IL-11, leading to high antagonist potency through competition with wild-type IL-11 for binding to IL-11Rα. Residues 79–84, which reside in loop AB of the hIL-11 structure, show increased temperature factors with respect to the adjacent residues of loop AB, and residues 83 and 84 show high disorder and were consequently omitted from the coordinates. These structural data suggest that the inherent flexibility of this region of loop AB may allow the mutated residues to form different and/or more extensive binding interactions with IL-11Rα than those of wild-type IL-11, mediating the higher affinity of this interaction. Our recent work demonstrated that this antagonist effectively inhibits IL-11-mediated activation of STAT3 and GI tumour progression *in vivo* (Putoczki *et al.*, 2013).

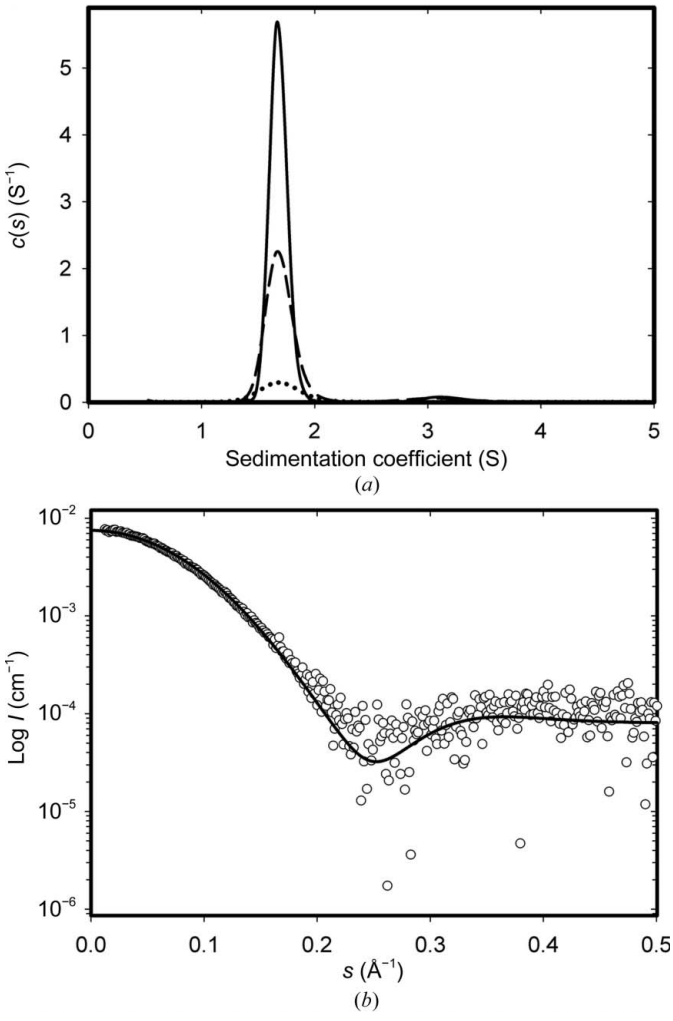

Figure 2
Solution structure analysis of hIL-11. (*a*) Continuous sedimenation-coefficient distributions for hIL-11 at 0.2 mg ml^{-1} (dotted line), 0.6 mg ml^{-1} (dashed line) and 1.0 mg ml^{-1} (solid line). (*b*) Small-angle X-ray scattering data (circles) are overlaid with the calculated scattering profile for the crystal structure of hIL-11 (solid line).

3.4. Structural comparison of hIL-11 with IL-6

IL-11 has been shown to form a hexameric complex comprising $(IL\text{-}11)_2$–$(IL\text{-}11R\alpha)_2$–$(GP130)_2$ (Barton *et al.*, 2000) that is thought to be analogous to the well characterized IL-6 signalling complex. Thus, much of the functional and mechanistic data generated for IL-11 have been interpreted in the context of the structure of the IL-6 signalling complex. However, a direct comparison of our structure of hIL-11 with that of IL-6 (PDB entry 1alu; Somers *et al.*, 1997) shows important structural differences between the two cytokines.

Alignment of the structures of hIL-11 and IL-6 based on secondary-structure matching and equivalent residue positions using *SUPERPOSE* (Krissinel & Henrick, 2004) confirms that the relative positioning of the four core helices and large loops are similar (Fig. 4*a*; see also Supplementary Fig. S5 for a sequence alignment). However, the core helical elements of hIL-11 are significantly longer than those of IL-6. In particular, helices C and D of hIL-11 contain 30 and 31 residues, respectively, as analysed by *DSSP*, while those of IL-6 contain 21 and 26 residues, respectively. This results in significant elongation of the IL-11 structure with respect to IL-6. In addition, hIL-11 lacks the α-helical segment in loop CD and the small segment of 3_{10}-helix in loop AB of IL-6.

3.5. Comparison of the receptor-binding sites of hIL-11 and IL-6

The program *PISA* (Krissinel & Henrick, 2007) was used to identify the residues of IL-6 that form interface contacts with IL-6Rα and the two molecules of GP130 in the crystal structure of the hexameric complex (PDB entry 1p9m; see Supplementary Figs. S4 and S6). Comparison of these binding interfaces with those that we have identified for IL-11 (Fig. 3) shows that the three sites are arranged similarly on the two molecules, supporting a similar spatial arrangement of the hexameric complex. However, with respect to IL-6 the helical extensions of IL-11 contain a number of residues previously identified as necessary for binding to IL-11Rα and the primary molecule of GP130 (sites I and II; Fig. 3). Thus, these IL-11 residues have no structural counterparts in IL-6.

Of particular interest are the regions of IL-11 that bind the two molecules of GP130 in the functional signalling complex. The structural alignment of the proteins allows the direct comparison of the residues of IL-6 that bind GP130 with their counterparts in the IL-11 structure (Supplementary Table S1). The residue-by-residue comparison of site II of IL-6 with the corresponding residues in IL-11 shows low conservation and only weak similarity of the interface residues. A striking difference is the presence of four arginine residues in helix C of IL-11 (positions 132, 135, 138 and 139) in the same positions as uncharged residues in IL-6. Three of these arginine residues have been verified experimentally as being important for IL-11 activity (Fig. 3*a*). Adjustment of the alignment by one helical turn, placing IL-6 towards the site II/III end (the N-terminal end of helix A) of IL-11 (Supplementary Table S1), does not significantly improve the agreement of these residues between the two cytokines.

The presence of these arginine residues creates a highly positively charged patch within site II of hIL-11. Comparison of the nature and distribution of surface electrostatic potential in hIL-11 and IL-6 (Fig. 4*b*) shows differences between the two cytokines. IL-11 shows a large area of positive surface potential in the region of site II, with the most highly charged areas on the surface of the molecule formed by helices A and C. In contrast, site II of IL-6 shows a more localized positive surface potential clustered near the N-terminal end of helix A.

The residue-by-residue comparison of site III of IL-6, which binds the second molecule of GP130 in the hexamer, with the corresponding residues of IL-11 shows stronger similarity between the two proteins (Supplementary Table S1). Of particular note is the conservation of Trp168 (Trp157 in IL-6), which is known to be crucial for GP130 binding by IL-11 and forms a central part of the binding interface in the IL-6 signalling complex. This suggests that the binding configuration and specific interactions of IL-11 and IL-6 with the second molecule of GP130 *via* site III are

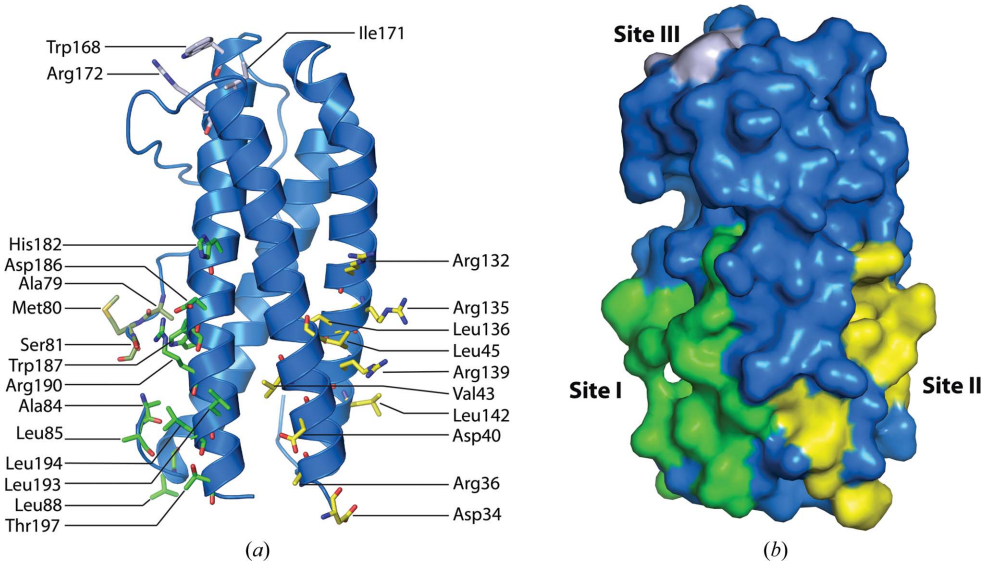

Figure 3
The receptor-binding regions of IL-11. (*a*) Residues identified as being involved in binding of IL-11Rα (green, site I) and GP130 (yellow, site II; grey, site III) are shown in stick representation. Residues 79–81 of loop AB, which are mutated in the high-affinity antagonist variant of IL-11, are shown in dark green (residues 82 and 83 were omitted from the model). Residue numbering is provided according to the full-length precursor sequence of IL-11. (*b*) Surface representation of hIL-11 showing the positions of the receptor-binding regions for IL-11Rα (green, site 1) and two molecules of GP130 (yellow, site II; grey, site III).

somewhat conserved between the two cytokines. Another notable structural feature in this region of hIL-11 is a section of 3_{10}-helix comprising the six N-terminal residues of helix C that is not present in IL-6. This strained helical structure is located directly adjacent to Trp168, hinting that this part of the protein may also play a functional role in complex formation with GP130 *via* site III.

Taken together, these data suggest that the binding mode of IL-11 to GP130 at site II is different from that of IL-6. Previous work has shown that IL-6 binds to the first molecule of GP130 at the hinge region between the two fibronectin type III domains of GP130 that make up the cytokine-binding module (CBM), while the second molecule of GP130 engages with the distal end of IL-6 (site III) and also forms contacts with the bound IL-6Rα (Supplementary Fig. S4). Both the elongation of IL-11 with respect to IL-6 and the involvement of the distal ends of the protein in binding of the two GP130 molecules have implications for the formation and configuration of the hexameric complex. Specifically, the distance between the two bound GP130 molecules may be significantly larger for IL-11 than is observed for IL-6. This may also affect any interactions of the second molecule of GP130 with IL-11Rα. It is possible that IL-11 binds to GP130 at a similar site to IL-6 but in a different orientation or with different molecular positioning of the cytokine on the cytokine-binding module of GP130. An alternative possibility is that rearrangement of the binding surface of GP130 is necessary in order to accommodate the chemically different IL-11 site II interface surface. Previous comparison of the crystal structures of GP130 in complex with leukaemia inhibitory factor, a viral IL-6 homologue, and human IL-6 indicated that the site II residues of each cytokine used to engage GP130 were divergent in both positioning and chemical nature (Boulanger, Bankovich *et al.*, 2003). This study also showed that the structure of the cytokine-binding site of GP130 remained relatively unchanged in all three structures and that the different cytokines utilize separate but overlapping binding sites on GP130. Our structural data suggest that this is also likely to be the case for IL-11 in comparison with IL-6. Importantly, early work demonstrated that monoclonal antibodies directed against different epitopes of GP130 resulted in specific inhibition of IL-6 signalling while leaving IL-11 signalling unchanged or *vice versa* (Gu *et al.*,

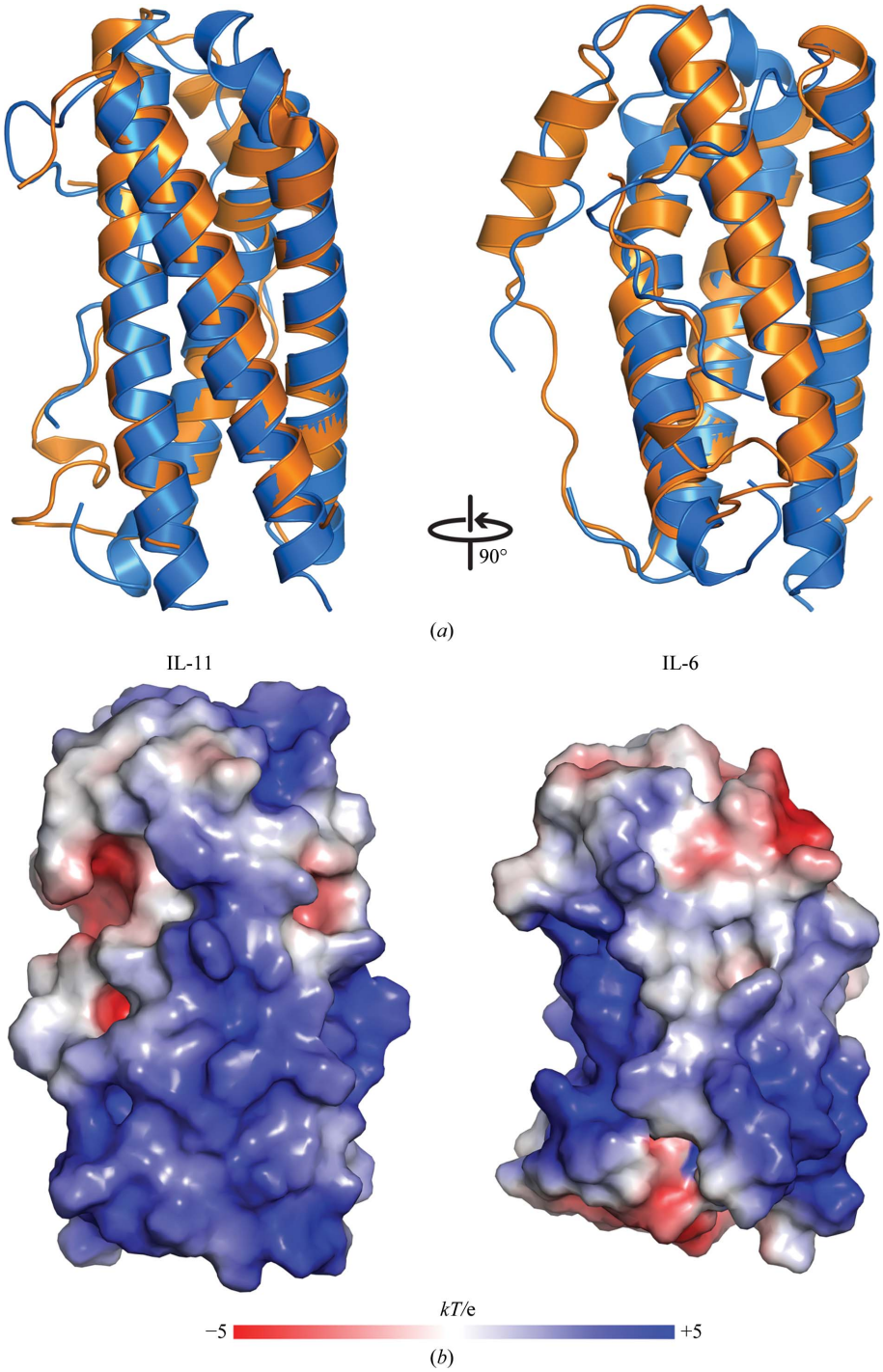

Figure 4
Structural comparison of hIL-11 with IL-6. (*a*) The crystal structure of IL-6 (PDB entry 1alu; orange) was aligned with the structure of hIL-11 (blue) using *SUPERPOSE*. The r.m.s.d. for 127 aligned C^{α} atoms was 1.59 Å. (*b*) Surface electrostatic potential for hIL-11 and IL-6 calculated using *APBS*. Both IL-11 and IL-6 are oriented as shown in Fig. 3, with site I on the left of the molecule and site II on the right (see Fig. 2 and Supplementary Fig. S6). Negative and positive electrostatic potential is contoured at $-5kT$/e (red) and $+5kT$/e (blue), respectively.

1996). Furthermore, mutational studies of the CBM of GP130 show that some residues of GP130 are involved in activation by both IL-11 and IL-6, while others are only required for activation by IL-11 and are not involved in activation by IL-6 (Dahmen *et al.*, 1998; Kurth *et al.*, 1999). Together, these data indicate that different regions of GP130 are critical for signalling by IL-11 and IL-6, and further support structurally distinct configurations of the functional hexameric signalling complexes of the two cytokines.

4. Conclusions

In addition to its originally described physiological role in haematopoiesis, IL-11 has now been shown to play a significant role in other disease processes through activation of the JAK/STAT pathway (Putoczki & Ernst, 2010). The identification of new physiological and pathological roles for IL-11 emphasizes the need for improved understanding of the mechanism of signalling used by this under-characterized cytokine.

We have solved the first crystal structure of hIL-11, which provides structural insight into previous structure–function studies of the protein and highlights key differences from IL-6. Given the dominance of IL-11 over IL-6 in GI cancers (Putoczki *et al.*, 2013), and potentially other diseases, the crystal structure will provide essential information for further interrogation of the functional mechanisms of IL-11 in comparison to IL-6. Importantly, given the clinical use of hIL-11 for treatment of thrombocytopaenia and the preclinical success of inhibition of IL-11 signalling in GI cancers, the crystal structure of hIL-11 provides a platform for the design of new and improved agonist and antagonist variants of the protein.

MDWG is the recipient of the C. R. Roper Fellowship and an Australian Research Council Postdoctoral Fellowship (project No. DP110103528). Parts of this research were undertaken at the MX2 and SAXS/WAXS beamlines of the Australian Synchrotron, Victoria, Australia. The authors wish to thank Professor Michael Parker for helpful advice and suggestions.

References

Adams, P. D. *et al.* (2010). *Acta Cryst.* D**66**, 213–221.
Baker, N. A., Sept, D., Joseph, S., Holst, M. J. & McCammon, J. A. (2001). *Proc. Natl Acad. Sci. USA*, **98**, 10037–10041.
Barton, V. A., Hall, M. A., Hudson, K. R. & Heath, J. K. (2000). *J. Biol. Chem.* **275**, 36197–36203.
Barton, V. A., Hudson, K. R. & Heath, J. K. (1999). *J. Biol. Chem.* **274**, 5755–5761.
Boulanger, M. J., Bankovich, A. J., Kortemme, T., Baker, D. & Garcia, K. C. (2003). *Mol. Cell*, **12**, 577–589.
Boulanger, M. J., Chow, D.-C., Brevnova, E. E. & Garcia, K. C. (2003). *Science*, **300**, 2101–2104.
Czupryn, M. J., McCoy, J. M. & Scoble, H. A. (1995). *J. Biol. Chem.* **270**, 978–985.
Dahmen, H., Horsten, U., Küster, A., Jacques, Y., Minvielle, S., Kerr, I. M., Ciliberto, G., Paonessa, G., Heinrich, P. C. & Müller-Newen, G. (1998). *Biochem. J.* **331**, 695–702.
Dams-Kozlowska, H., Kwiatkowska-Borowczyk, E., Gryska, K. & Mackiewicz, A. (2013). *Int. J. Med. Sci.* **10**, 1157–1165.
Du, X. & Williams, D. A. (1997). *Blood*, **89**, 3897–3908.
Emsley, P., Lohkamp, B., Scott, W. G. & Cowtan, K. (2010). *Acta Cryst.* D**66**, 486–501.
Evans, P. R. (2011). *Acta Cryst.* D**67**, 282–292.
Evans, P. R. & Murshudov, G. N. (2013). *Acta Cryst.* D**69**, 1204–1214.
Garbers, C. & Scheller, J. (2013). *Biol. Chem.* **394**, 1145–1161.
Gu, Z.-J., Wijdenes, J., Zhang, X.-G., Hallet, M.-M., Clement, C. & Klein, B. (1996). *J. Immunol. Methods*, **190**, 21–27.
Harmegnies, D., Wang, X.-M., Vandenbussche, P., Leon, A., Vusio, P., Grötzinger, J., Jacques, Y., Goormaghtigh, E., Devreese, B. & Content, J. (2003). *Biochem. J.* **375**, 23–32.
Herrlinger, K. R., Witthoeft, T., Raedler, A., Bokemeyer, B., Krummenerl, T., Schulzke, J. D., Boerner, N., Kueppers, B., Emmrich, J., Mescheder, A., Schwertschlag, U., Shapiro, M. & Stange, E. F. (2006). *Am. J. Gastroenterol.* **101**, 793–797.
Kabsch, W. (2010). *Acta Cryst.* D**66**, 125–132.
Kabsch, W. & Sander, C. (1983). *Biopolymers*, **22**, 2577–2637.
Krissinel, E. & Henrick, K. (2004). *Acta Cryst.* D**60**, 2256–2268.
Krissinel, E. & Henrick, K. (2007). *J. Mol. Biol.* **372**, 774–797.
Kurth, I., Horsten, U., Pflanz, S., Dahmen, H., Küster, A., Grötzinger, J., Heinrich, P. C. & Müller-Newen, G. (1999). *J. Immunol.* **162**, 1480–1487.
Laue, T. M., Shah, B. D., Ridgeway, T. M. & Pelletier, S. L. (1992). *Analytical Ultracentrifugation in Biochemistry and Polymer Science*, edited by S. E. Harding, A. J. Rowe & J. C. Horton, pp. 90–125. Cambridge: Royal Society of Chemistry.
Lee, C. G., Hartl, D., Matsuura, H., Dunlop, F. M., Scotney, P. D., Fabri, L. J., Nash, A. D., Chen, N.-Y., Tang, C.-Y., Chen, Q., Homer, R. J., Baca, M. & Elias, J. A. (2008). *Am. J. Resp. Cell. Mol. Biol.* **39**, 739–746.
Matadeen, R., Hon, W. C., Heath, J. K., Jones, E. Y. & Fuller, S. (2007). *Structure*, **15**, 441–448.
McCoy, A. J., Grosse-Kunstleve, R. W., Adams, P. D., Winn, M. D., Storoni, L. C. & Read, R. J. (2007). *J. Appl. Cryst.* **40**, 658–674.
Murshudov, G. N., Skubák, P., Lebedev, A. A., Pannu, N. S., Steiner, R. A., Nicholls, R. A., Winn, M. D., Long, F. & Vagin, A. A. (2011). *Acta Cryst.* D**67**, 355–367.
Ortega, A., Amorós, D. & García de la Torre, J. (2011). *Biophys. J.* **101**, 892–898.
Peterson, R. L., Wang, L., Albert, L., Keith, J. C. & Dorner, A. J. (1998). *Lab. Invest.* **78**, 1503–1512.
Petoukhov, M. V., Franke, D., Shkumatov, A. V., Tria, G., Kikhney, A. G., Gajda, M., Gorba, C., Mertens, H. D. T., Konarev, P. V. & Svergun, D. I. (2012). *J. Appl. Cryst.* **45**, 342–350.
Putoczki, T. & Ernst, M. (2010). *J. Leukoc. Biol.* **88**, 1109–1117.
Putoczki, T. L. *et al.* (2013). *Cancer Cell*, **24**, 257–271.
Qiu, B. S., Pfeiffer, C. J. & Keith, J. C. (1996). *Dig. Dis. Sci.* **41**, 1625–1630.
Sands, B. E., Winston, B. D., Salzberg, B., Safdi, M., Barish, C., Wruble, L., Wilkins, R., Shapiro, M. & Schwertschlag, U. S. (2002). *Aliment. Pharmacol. Ther.* **16**, 399–406.
Schuck, P. (2000). *Biophys. J.* **78**, 1606–1619.
Schwertschlag, U. S., Trepicchio, W. L., Dykstra, K. H., Keith, J. C., Turner, K. J. & Dorner, A. J. (1999). *Leukemia*, **13**, 1307–1315.
Somers, W., Stahl, M. & Seehra, J. S. (1997). *EMBO J.* **16**, 989–997.
Svergun, D. I. (1992). *J. Appl. Cryst.* **25**, 495–503.
Svergun, D., Barberato, C. & Koch, M. H. J. (1995). *J. Appl. Cryst.* **28**, 768–773.
Tacken, I., Dahmen, H., Boisteau, O., Minvielle, S., Jacques, Y., Grötzinger, J., Küster, A., Horsten, U., Blanc, C., Montero-Julian, F. A., Heinrich, P. C. & Müller-Newen, G. (1999). *Eur. J. Biochem.* **265**, 645–655.
Taga, T. & Kishimoto, T. (1997). *Annu. Rev. Immunol.* **15**, 797–819.
Tanaka, T., Narazaki, M. & Kishimoto, T. (2012). *Annu. Rev. Pharmacol.* **52**, 199–219.

Underhill-Day, N., McGovern, L. A., Karpovich, N., Mardon, H. J., Barton, V. A. & Heath, J. K. (2003). *Endocrinology*, **144**, 3406–3414.
Winn, M. D. *et al.* (2011). *Acta Cryst.* D**67**, 235–242.
Yao, X., Huang, J., Zhong, H., Shen, N., Faggioni, R., Fung, M. & Yao, Y. (2014). *Pharmacol. Ther.* **141**, 125–139.